包覆钎料铝－钢螺柱焊接头组织及性能

葛佳棋， 蒋　勇， 王克鸿
（南京理工大学 材料科学与工程学院，南京　210094）

摘　要：采用包覆钎料感应加热方法，以 AlSi 钎料作为焊缝填充金属，对 Q235 钢螺柱和6061 铝合金进行钎焊．利用光学显微镜、扫描电镜、能谱分析等表征方法，对接头的组织、成分和相组成等进行了分析．结果表明，AlSi 钎料与铝母材反应充分，Si 元素扩散至铝母材形成针叶状的共晶组织，焊缝近钢侧生成一条狭窄连续的 Fe-Al 金属间化合物，并沿垂直于铝基体的方向生成出胞状晶，金属间化合物层由 Fe_2Al_5 和 $FeAl_3$ 的混合相组织组成．力学性能测试表明，接头的抗剪强度最大为65 MPa，近钢侧金属间化合物的显微硬度值较高，接头断裂在金属间化合物区域，属于延性断裂．

关键词：感应加热钎焊；异种金属焊接；微观组织；金属间化合物
中图分类号：TG406　　**文献标识码**：A　　**文章编号**：0253－360X(2012)07－0097－04

葛佳棋

0　序　　言

近年来，异种金属之间连接的应用越来越广泛．单一金属本身不可能满足应用所需的所有物理、化学和力学方面的性能，而异种金属接头可以满足需求，另外还可以节省费用，节约能源[1]．异种金属的组合螺柱焊问题，对于铝和钢组合使用表现得尤为明显．但由于铝与钢两者之间热物理性能差异大、铁在铝中的固溶度几乎为零[2]，铁在共晶温度下的极限溶解度为0.052%，并随着温度的下降而急剧减小且铁与铝可以产生多种硬而脆的金属间化合物，如 FeAl，$FeA1_2$，$FeA1_3$，Fe_2A1_5，Fe_2A1_7及 Fe_4Al_{13} 等，这些金属间化合物的存在，增加了焊接接头的脆性，降低了其塑性和韧性，严重恶化了接头的力学性能，这已成为铝钢螺柱焊接的难点问题[3－7]．由于电弧焊的热输入非常高，钢与铝都很容易熔化，很难控制熔合区金属间化合物层的成分，导致脆性金属间化合物层的严重长大[8]，所以难以采用电弧焊的方法焊接钢和铝．

钎焊作为一种非熔化焊的焊接方法，利用钎料在低于母材固相线但高于钎料液相线的温度下发生熔化，能够在铝钢母材表面润湿、铺展、填缝，与母材发生相互溶解扩散[9]，并能在一定程度上抑制Fe-Al金属间化合物的生成，能基本满足对铝钢焊缝的要求[10]．文中采用感应加热钎焊的方法焊接钢螺柱与铝板，进一步研究焊接接头的组织性能．

1　试验条件

试验选用6061 铝板（80 mm × 80 mm × 12 mm），钢螺柱母材选用 Q235 棒材，尺寸为长 55 mm，底面直径16 mm．熔敷金属采用了自制的 AlSi 箔带，焊接过程采用自制铝－钢熔敷焊保护剂，并设计了箔带包裹保护剂预装模式，进行熔敷填充．各试验材料具体成分及力学性能见表1．铝板采用丙酮除油处理后，用 NaOH 溶液去除表面氧化膜，钢螺柱采用丙酮作除油处理．

表1　铝板、钢螺柱母材化学成分（质量分数，%）与抗剪强度

Table 1　Chemical compositions and mechanical properties of aluminum base metal and steel stud

材料	Si	C	Cu	Mn	Mg	Cr	Zn	S	Zn	Ti	P	Ni	Fe	Al	抗剪强度 R_τ/MPa
6061	0.4~0.8	—	0.15~0.4	0.15	0.8~1.2	0.04~0.35	0.25	—	0.25	0.15	—	—	0.7	余量	85
Q235	≤0.30	≤0.18	—	0.35~0.80	—	0.70	—	0.04	—	—	0.04	0.021	余量	—	—

收稿日期：2011－12－31

2 试验方法

将 AlSi 箔带与自制铝-钢熔敷焊保护剂进行包覆,制成外层为箔带,里层为铝-钢熔敷焊保护剂的药芯焊丝包覆钎料;包敷钎料采用缠绕的方式预置在螺柱周边.

感应器的结构设计如图 1 所示,感应线圈的外径为 80 mm,内径为 40 mm,线圈厚度为 15 mm,调节离铝板表面的高度为 2 mm. 试验中使用的焊接工艺参数为感应器电流 900 A,加热时间 150 s.

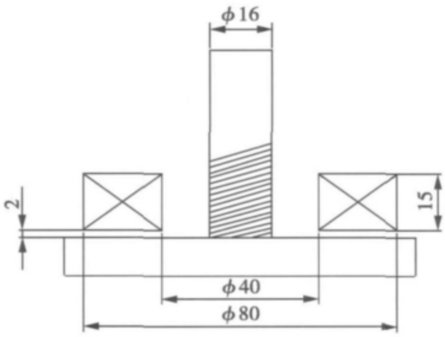

图 1 待焊示意图(mm)
Fig. 1 Diagram of form of welded joints

制备金相试样,使用 OLYMPUSBX60M 金相显微镜进行接头内部组织的观察,Hitachi X-650 扫描电子显微镜进行微观组织观察和元素分析,HVS-1000Z 显微硬度计对焊接试样进行显微维氏硬度测试.

3 试验结果与分析

3.1 焊缝组织和成分分析

图2 为 Al-Si 钎料铝-钢螺柱钎焊试样的宏观形貌. 可以看出焊缝成形良好,焊接过程中钎料全部熔化,铺展情况较好,由于钎料熔化后继续加热了一段时间,保证了钎料在铝钢母材之间的充分渗透.

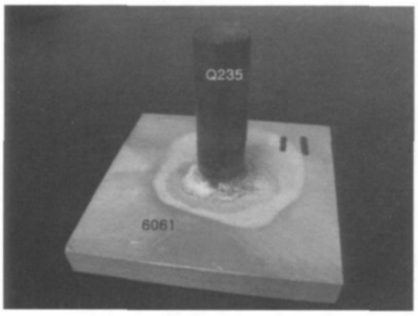

图 2 焊接试样宏观形貌
Fig. 2 Welding joints

将试样沿螺柱直径方向线切割,得到钢螺柱与铝板接头的剖面. 图 3 为钎焊接头的金相组织. 上侧为钢母材,下侧为铝基体,接头连接较为致密,钎缝组织由 Fe-Al 金属间化合物、Al-Si 共晶相、α-Al 固溶体三个区域组成. 由图 3 中可以看出,钢侧形成一条比较平的直线,而 AlSi 钎料与铝母材反应充分,钎料中的铝与铝母材混合形成铝基体;在钎料温度达到固相线开始熔化后,与铝母材接触,硅向铝母材中扩散,形成针叶状的 Al-Si 共晶组织,此时的钢螺柱并未熔化,铁还处于固态,所以一旦富铝的液相组织形成,Fe 元素便快速地扩散熔入液相并与之发生反应,形成熔点较高的 Fe-Al 金属间化合物,从而液相会消失;由于铝冷却速度较快,金属间化合物沿垂直于铝基体的方向生成出一些胞状晶.

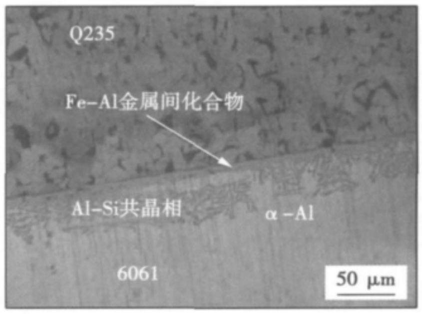

图 3 焊缝金相组织
Fig. 3 Microstructure of welding seam

图 4 为金属间化合物区域放大的 EDS 形貌. 能谱分析表明图 4 中谱图 1 所在浅灰色区域为连续的 Fe-Al 金属间化合物带,其中 Al 元素含量为 70.99%(原子分数,下同),Fe 元素含量为 15.72%,Si 元素含量为 13.29%;在谱图 2 区域 Al 元素含量为 97.50%,Fe 元素含量为 0.74%,Si 元素含量为 1.77%. 结合 Al-Fe 二元相图,可以推断谱图 1 区组织为 Fe_2Al_5 和 $FeAl_3$ 的混合相组织,同时还有少量 α-Al 组织;谱图 2 区为 Al-Si 共晶组织和少量 $FeAl_3$ 的混合相组织. 金属间化合物厚度大致为 10 μm,由图 3 中可以看出,金属间化合物厚度占整个钎焊对接接头厚度的 15% ~20%.

图 5 为钎焊焊缝的线扫描结果,从铁基体到 Fe-Al 化合物区域,Fe 元素的含量逐渐减少到最低,之后 Fe 元素出现细微地增加,这是 Fe 原子向铝的液相组织熔融和扩散的结果,而 Al 元素在金属化合物区间富集,靠近铁基体界面处迅速减少,只有极少量扩散至铁基体当中,这是由于 Fe 原子是在液相铝中

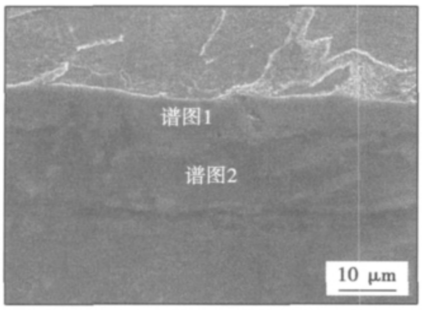

图 4　金属间化合物层的扫描电镜形貌
Fig. 4　SEM photo in intermetallic compounds zone

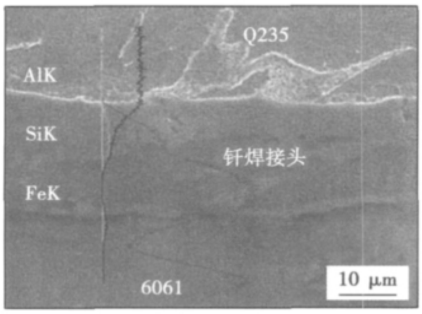

图 5　接头线扫描结果
Fig. 5　Line scan results of welding seam

扩散,而 Al 原子是向固体铁中扩散的原故,同时 Si 元素含量在近铁基体方向有略微增加. 熔融和扩散到液相铝中的 Fe 元素与铝生成连续的 Fe_2Al_5 和 $FeAl_3$ 等金属间化合物.

3.2　力学性能测试分析

固定焊接试样的铝板,沿平行于铝板的方向,在螺柱根部进行剪切,测试其抗剪强度. 试验过程中感应器电流调至 900 A,采用不同的焊接时间得到不同抗剪强度. 焊接 150 s 时钎料在母材之间渗透扩散较好,抗剪强度最高为 65 MPa,达到 6061 母材抗剪强度的 76.5%; 当焊接时间过低时,钎料还未完全渗透就停止加热,导致钎料与母材结合不牢固; 焊接时间过长时,会导致熔融钎料从钎缝流走,还可能产生熔蚀现象,使得铝板表面留下麻面或凹坑,这些都会造成焊接接头强度的下降. 试验结果见表 2 (表 2 中抗剪强度为多个试样测试结果的平均值) .

图 6 给出的是焊缝显微硬度曲线,在焊缝接头区域及两边的母材,沿同一条直线每隔 0.02 mm 取一点进行显微硬度测试. 从图 6 中可以看出,焊缝两侧母材的硬度值分布较为均匀,钢侧平均硬度为 131.9 HV,铝侧平均硬度为 47.9 HV. 焊缝近钢侧区的显微硬度最高为 445.6 HV,向铝侧方向焊缝区域的硬度呈明显的降低趋势. 这是由于焊接过程中

表 2　焊接时间与抗剪强度的对比关系
Table 2　Comparison between welding time and shear strength

编号	感应器电流 I/A	焊接时间 t/s	抗剪强度 R_τ/MPa	6061 母材抗剪强度 $R_{\tau m}$/MPa	强度系数 A(%)
1	900	140	53	85	62.4
2	900	150	65	85	76.5
3	900	160	64	85	75.3
4	900	170	50	85	58.8

铁融入液态的钎料,即铝硅共晶相中与之发生反应生成 Fe_2Al_5 和 $FeAl_3$,这两种金属间化合物都是脆性大硬度高. 随着 Fe 元素含量向铝母材方向上的降低,生成的金属间化合物逐渐减少,硬度逐渐降低; 在焊接接头近铝侧区域成分为 Al-Si 共晶组织,金相呈细长的针叶状,硬度比铝母材稍高.

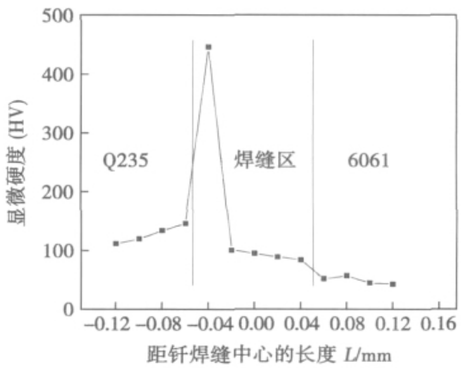

图 6　接头显微硬度
Fig. 6　Microhardness of welding joints

3.3　断口分析

图 7 为断口的 EDS 的分析形貌,其中方框 1 中成分 F 元素含量为 60.64%(原子分数,下同) ,K 元素含量为 13.19% ,Al 元素含量为 22.44% ,Si 元素含量为 0.75% ,Fe 元素含量为 0.59%. 在钢螺柱的断面上留有白色岛状物质,主要是钎剂遗留下的 F

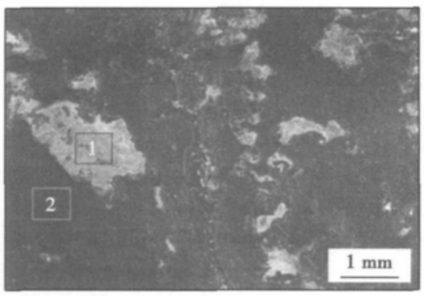

图 7　接头断口形貌
Fig. 7　Fracture morphology of welded joint

元素和 K 元素; 方框 2 中成分 Al 元素含量为 54.44%,Fe 元素含量为 40.89%,Si 元素含量为 4.48%,Mn 元素含量为 0.18%. 结合 Fe-Al 二元相图,可判断方框 1 中还含有少量的 $FeAl_3$,方框 2 处为 Fe_2Al_5 和 $FeAl_3$ 等金属间化合物.

图 8 为不同放大倍数的断口形貌,其中图 8a 可以看到断口表面比较复杂,仍有少量的白色岛状物质残留,为钎焊结束后残余的保护剂; 图 8b 可以看到大量形貌为纤维状的长条组织,并且出现少量不同高度的台阶. 结合断口的成分可以判断,这种断裂属于延性断裂,纤维状长条组织为平行于断口方向的剪切力与垂直于断面的拉伸力产生的拉拔作用所致,断裂面发生在金属间化合物区域.

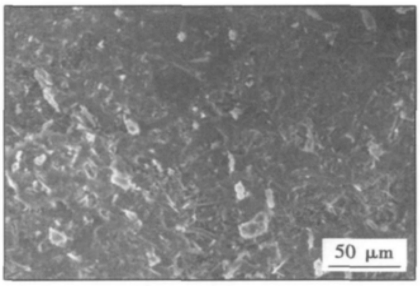

(a) 500倍断口形貌

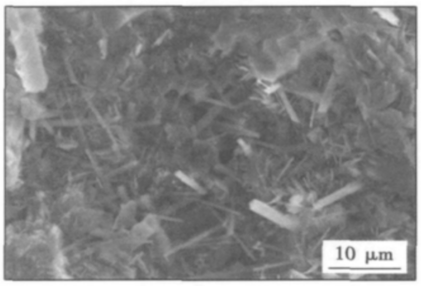

(b) 2 000倍断口形貌

图 8 接头断口形貌

Fig. 8 Fracture morphology of welded joint

4 结 论

(1) 采用 AlSi 钎料,以感应加热钎焊方法焊接 Q235 钢螺柱和 6061 铝合金,能够得到良好的焊接接头,接头组织由金属间化合物 Fe_2Al_5 和 $FeAl_3$、Al-Si 共晶相、α-Al 固溶体三个区域组成. 金属间化合物厚度为 10 μm 左右.

(2) 剪切试验表明,焊缝接头在金属间化合物区间断裂,断裂性质为延性断裂,最大抗剪强度为 65 MPa,达到 6061 母材抗剪强度的 76.5%.

(3) 焊缝接头金属间化合物区域显微硬度最大为 445.6 HV,近铝侧区域呈细长的针叶状 Al-Si 共晶组织,硬度比铝母材稍高.

参考文献:

[1] 杨雷亭, 杨师斌. 异种金属材料的焊接[J]. 煤矿机械, 2008, 29(6): 102-104.
Yang Leiting, Yang Shibin. Welding of different metal materials [J]. Coal Mine Machinery, 2008, 29(6): 102-104.

[2] Peyre P, Sierra G, Deschaux-Beaume F, *et al*. Generation of aluminium-steel joints with laser-induced reactive wetting [J]. Materials Science and Engineering, 2007, 444: 327-338.

[3] Takehiko W, Hirofumi T, Atsushi Y. Joining of aluminum alloy to steel by friction stir welding[J]. Journal of Materials Processing Technology, 2006, 178: 342-349.

[4] Alexandre M, Rajashekar S, Alexis D, *et al*. Dissimilar material joining using laser[J]. Optics & Laser Technology, 2007, 39: 652-661.

[5] 雷 振, 秦国梁, 王旭友, 等. 铝/镀锌钢复合热源熔-钎接头的局部"未钎合"缺陷分析[J]. 焊接学报, 2007, 28(10): 37-41.
Lei Zhen, Qin Guoliang, Wang Xuyou, *et al*. Analysis for local incomplete brazing in fusion-brazed joints between aluminium and zinc-coated steel by hybrid welding[J]. Transactions of the China Welding Institution, 2007, 28(10): 37-41.

[6] 石常亮, 何 鹏, 冯吉才, 等. 铝/镀锌钢板 CMT 熔钎焊界面区组织与接头性能[J]. 焊接学报, 2006, 27(12): 61-64.
Shi Changliang, He Peng, Feng Jicai, *et al*. Interface microstructure and mechanical property of CMT welding-brazed joint between aluminum and galvanized steel sheet[J]. Transactions of the China Welding Institution, 2006, 27(12): 61-64.

[7] Rattana B, Taisei Y, Yukio M, *et al*. Suppression of intermetallic reaction layer formation by controlling heat flow in dissimilar joining of steel and aluminum alloy [J]. Materials Science and Engineering, 2007, 467: 108-113.

[8] 雷 振, 王旭友, 王伟波, 等. 铝/镀锌钢复合热源熔—钎接头中的 Al-Fe 金属间化合物层分析[J]. 焊接学报, 2007, 28(11): 65-68.
Lei Zhen, Wang Xuyou, Wang Weibo, *et al*. Analysis for Al-Fe intermetallic compounds layer of fusion-brazed joints between aluminium and zinc-coated steel by hybrid welding[J]. Transactions of the China Welding Institution, 2007, 28(11): 65-68.

[9] 周万盛, 姚君山. 铝及铝合金的焊接[M]. 北京: 机械工业出版社, 2006.

[10] 刘师田, 杨凯珍. 保温时间和钎焊温度对真空钎焊 304 不锈钢接头性能的影响[J]. 金属铸锻焊技术, 2011, 40(5): 172-174.
Liu Shitian, Yang Kaizhen. Effect of holding time and brazing temperature on microstructure and mechanical properties of 304 stainless steel brazed joints[J]. Hot Working Technology, 2011, 40(5): 172-174.

作者简介: 葛佳棋, 男, 1986 年出生, 博士研究生. 主要从事铝钢异种金属焊接. 发表论文 1 篇. Email: messiah35@sina.com

通讯作者: 王克鸿, 男,博士研究生导师. Email: wkh1602@126.com

ing temperature increasing. It also increased with strain rate decreasing. Average grain size increased with straining, and with forming temperature increasing.

Key words: microstructure evolution; laser welding; superplastic deformation

Microstructure and properties of dissimilar materials Mg/Al laped joint by friction stir welding

CHEN Ying, FU Ningning, SHEN Chenbin, GE Jiping (School of Materials Science and Engineering, Dalian Jiaotong University, Dalian 116028, China). pp 93 – 96

Abstract: 5083 aluminum alloy and AZ31 magnesium alloy were lap jointed by using friction stir lap welding. The mechanical properties, microstructure and fracture appearance of the joint were investigated. The results indicated that a high shear strength, interface bonding and defect-free weld have been obtained when the probe of a tool did not contact the lower Mg sheet and the suitable welding parameters are used. 5083 and AZ31 were jointed by a conversion layer that existed in interface zone which contained intermetallic compounds. The joints fractured in interface. Fractographs confirm that the fracture of the Al side is composed of the "small pit" by plastic tearing, but the fracture of the Mg side consists of river line pattern mainly. The micro hardness raised in the interface zone.

Key words: friction stir lap welding; magnesium alloy; aluminum alloy; conversion layer

Microstructure characteristics and properties of steel stud to aluminum alloy made by covering filler metal brazing

GE Jiaqi, JIANG Yong, WANG Kehong (School of Material Science and Engineering, Nanjing University of Science and Technology, Nanjing 210094, China). pp 97 – 100

Abstract: Q235 steel stud and 6061 aluminum alloy with AlSi as filler metal were joined by using high-frequency induction brazing. Microstructure, composition and phase composition of the welded joint were characterized by optical microscopy, SEM, EDAX EDS diffraction analysis. The results showed that AlSi filler completely reacted to 6061 aluminum base metal, needle-like eutectic was formed with the diffusion of Si to aluminum base metal; continuous Fe-Al intermetallic compounds which should be composed of Fe_2Al_5 and $FeAl_3$ generated near the steel side in the brazing seam, and some cellular crystal generated along the direction perpendicular to the Al base metal. Mechanical properties tests showed that the shear strength of welding joint was up to 65 MPa, fracture occurred in the Fe-Al intermetallic compounds where the microhardness was high. Fracture properties belonged to ductile fracture.

Key words: high-frequency induction brazing; dissimilar metal welding; microstructure; intermetallic compounds

Research on laser spot weld-bonding process characteristics

WANG Mingmao[1], TAO Wang[1], MA Yinan[1], CHEN Yanbin[1], WANG Yang[2] (1. State Key Laboratory of Advanced Welding and Joining, Harbin Institute of Technology, Harbin 150001, China; 2. School of Mechatronics Engineering, Harbin Institute of Technology, Harbin 150001, China). pp 101 – 104

Abstract: The stability of the laser spot weld-bond is analyzed and the exhaust means of the gas from the adhesives with different properties are studied. The weld defects of laser spot weld-bonding process are solved. The key of the weld-bonding process is the appropriate exhaust path for the gas from the adhesive decomposition, the plate gap is an important exhaust channel. The greater the adhesive viscosity is, the worse the weldability is. For the low viscosity adhesive, a reliable connection can be got by the slow rising laser pulse welding technology; for the large viscosity adhesive, a reliable connection can be achieved by filler wire and using the laser spike pulse welding process. The welding process can solve the weld defects of different viscosity adhesive, expanding the applications of the laser weld-bonding technology.

Key words: laser spot weld-bond; adhesive layer; viscosity; spatter; pulse

Microstructure in linear friction welded dissimillar titanium alloy joint

LANG Bo, ZHANG Tiancang, TAO Jun, GUO Delun (Beijing Aeronautical Manufacturing Technology Research Institute, Beijing 100024, China). pp 105 – 108, 112

Abstract: Microstructure at the different zones of linear friction welded TC11 and TC17 dissimillar titanium alloy joint were investigated to understand the mechanism of microstructural formation in the joints. The results showed that four different structures existed in linear friction welded joint, i. e. thermomechanically affected zone (TMAZ) in the region close to TC11 parent material, TMAZ the region close to TC17 parent material, weld zone in the region close to TC11 TMAZ, and weld zone in the region close to TC17 TMAZ. Although no dynamic recrystallization was observed in the TMAZ, the phase transformation would occur concurrently with material deformation during welding. In contrast, dynamic recrystallization occurred in the weld. Common prior-beta grains were formed at the original rubbing interface after welding. Under the conditions of 3 mm amplitude of oscillation, 40 Hz frequency of oscillation, 66.7 MPa friction pressure and absence of forge force, prior-beta grain size and alpha plate width increased with friction time increasing.

Key words: titanium alloy; linear friction welding; microstructure

Weld defect segmentation and extraction of X-ray image based on B-spline curve

LIANG Peng, WEI Yanhong, ZHAN Xiaohong (College of Material Science and Technology, Nanjing University of Aeronautics and Astronautics, Nanjing 211100, China). pp 109 – 112

Abstract: Aiming at the facts that most X-ray digital images have the problem of low contrast, large background fluctuation and complex texture, b-spline curve is used to fit the column gray curves after preprocessing of weld images. The result shows that redundant curve peaks are eliminated and a smooth curve is abtained. Furthermore, curve extreme points are extracted and extreme value point set is modified twice by a fluctuation threshold and a boundary threshold. Finally, the shape and size of defects are revised by mathematical morphology and median filtering. Experiment results shows that this strategy effectively solves the problem of defect extraction caused by the weld seam with complex texture in X-ray image. It is advantageous to realize the automatic extraction of weld defects in X-ray image.

Key words: spline curve; weld defect; image processing